Oceanological and Hydrobiological Studies

International Journal of Oceanography and Hydrobiology

Volume 54, No. 2 July 2025
pages (138-159)

sciendo

ISSN 1730-413X
eISSN 1897-3191

Geochemistry and provenance of core sediments from the southwestern Okinawa Trough

by

Kuo-Ming Huang[1], Yung-Tan Lee[2,*], I-An Chang[3], Ren-Yi Huang[4], Meng-Lung Lin[5], Yen-Tsui Hu[2]

DOI: **https://doi.org/10.26881/oahs-2025.1.12**
Category: **Original research paper**
Received: **March 27, 2025**
Accepted: **June 24, 2025**

[1]*Department of Applied Geomatics, Chien Hsin University, Taoyuan City, Taiwan, ROC*
[2]*Department of Tourism and Travel Management, Taipei University of Marine Technology, New Taipei City, Taiwan, ROC*
[3]*Institute of Oceanography , National Taiwan University, Taipei, Taiwan, ROC*
[4]*Department of Leisure Business Management, Hungkuo Delin University of Technology, New Taipei City, Taiwan, ROC*
[5]*Department of Tourism, Aletheia University, New Taipei City, Taiwan, ROC*

* Corresponding author: *yungtan@mail.tumt.edu.tw*

Abstract

Understanding the sedimentary processes and provenance in the Okinawa Trough is critical for reconstructing regional tectonic evolution and sediment transport dynamics in this active back-arc basin. This study focuses on the geochemical characteristics of cored sediments from the southwestern Okinawa Trough to investigate their depositional processes and sediment source contributions. Geochemical analysis, including major and trace element concentrations as well as rare earth element (REE) patterns, reveals that REEs are predominantly associated with clay minerals, indicating their key role in sediment transport and diagenesis. La–Th–Sc ternary plots suggest a mixed provenance, with sediment contributions from northeastern Taiwan, the East China Sea continental shelf, and volcanic material from the Okinawa Trough. A three-end-member mixing model was applied to estimate the relative contributions of these sources. Results indicate that sediments from the Lan-Yang area in northeastern Taiwan account for approximately 54.63% of the total input, followed by 24.12% from the East China Sea shelf and 21.25% from local volcanic sources. The spatial distribution of source contributions further reflects the influence of fluvial input and ocean currents on sediment dispersal. These findings offer new insights into sedimentary processes and tectonic activity in the region.

Key words: Rare earth elements, Clay mineral adsorption, Back-arc basin sedimentation, Mixing model analysis, Terrigenous input

1. Introduction

The Okinawa Trough is situated in the western Pacific, between the East China Sea continental shelf and the Ryukyu Island Arc. It extends northward toward the Japanese archipelago and connects southward to the northeastern offshore region of Taiwan, trending from north-northeast to south-southwest. Based on its geographic position, morphology, and sediment thickness, the trough is subdivided into three sectors: northern, central, and southern sub-basins. In the northeastern offshore region of Taiwan, the Philippine Sea Plate subducts beneath the Eurasian Plate, forming the Ryukyu Trench–Arc system. Within this tectonic framework, the Okinawa Trough is recognized as a back-arc rift basin (Lee et al., 1980; Letouzey & Kimura, 1985; Sibuet et al., 1987).

The trench reaches depths exceeding 1000 m, becoming progressively deeper toward the south, with the maximum depth—between 2000 m and 2270 m—located in its southwestern sector. Sediments in the Okinawa Trough predominantly consist of terrigenous clastic material, biogenic remains (e.g., shell fragments), and volcanic detritus. Grain size generally decreases from north to south, whereas the abundance of volcanic material increases northward. Ujiie (1994) proposed that the Okinawa Trough began forming approximately 1.7–0.5 million years ago and is currently in an early extensional stage. Since the Miocene, the region has experienced three major episodes of extension: around 9–6 Ma, 2 Ma, and from 0.1 Ma to the present (Furukawa et al., 1991). The latest phase of rifting is marked by a ~5 km wide zone of active deformation, with a total estimated extension of ~30 km (Sibuet et al., 1995, 1998).

Fairbanks (1989) suggested that during the last glacial maximum, a ~120 m drop in sea level (Ujiie et al., 1991) transformed the previously open marine environment into a semi-enclosed basin. The southern Okinawa Trough (SOT) is characterized by intense tectonic activity, including numerous normal faults, grabens, and active volcanic centers (Luo, 2001). Volcanism in this region remains ongoing. The southernmost Ryukyu Arc has undergone significant southward migration (Chen et al., 2017; Hsu, 2001), and the associated back-arc rifting in the SOT is particularly dynamic, featuring active hydrothermal systems and frequent seismic events (Lin et al., 2009).

Lin and Chen (1983) analyzed the grain size distribution and mineral composition of sediments from the Okinawa Trough and identified multiple provenance sources, including the Yangtze River, Taiwan, and the Ryukyu Islands. Lin (1992) further examined the physical properties and clay mineralogy of surface sediments in the northeastern offshore region of Taiwan, proposing the Lanyang River as a significant contributor to sediment input in the SOT.

Terrigenous clastic material in the Okinawa Trough is predominantly concentrated outside submarine canyons, where it forms submarine fan deposits. These fans are associated with canyon systems and are characterized by gentle topography, high terrigenous content, and substantial sediment flux, indicating that submarine canyons serve as important conduits for delivering terrestrial sediments into the trough (Li et al., 2001).

The distribution and composition of suspended particles in the central and SOT are influenced by several factors, including the Kuroshio Current—which acts as a barrier to sediment transport from the East China Sea continental shelf into the trough—biological productivity, regional bathymetry, and local geographical conditions (Guo et al., 2001). Suspended particle concentrations in the SOT generally decrease with increasing distance from the shoreline but increase with depth (Chung & Hung, 2000), a pattern attributed to resuspension processes and ocean current transport (Hung et al., 1999).

Based on a comprehensive analysis of depositional factors and regional stratigraphy in the SOT, Hu et al. (2019) concluded that the sediments in the SOT primarily derive from the weathering and erosion of sedimentary and metasedimentary rocks located in western and northeastern Taiwan. These source rocks encompass a diverse lithological range. Previous studies (Lou & Chen, 1996; Shieh et al., 1997; Ujiie & Ujiie 1999) estimate the Holocene sedimentation rate in the SOT to be approximately 20 cm/kyr.

There are two prevailing hypotheses regarding sediment provenance in the Okinawa Trough. One posits that sediments are primarily transported from Mainland Rivers, such as the Yangtze and Yellow Rivers, across the East China Sea continental shelf (Chung & Hung, 2000; Hsu et al., 1998; Kao et al., 2003). The alternative view emphasizes the Lanyang River in eastern Taiwan as the dominant sediment source (Chen & Kuo, 1980; Wang et al., 1985).

This study focuses on the southern segment of the Okinawa Trough, with sampling stations located between 122.5°E and 125°E longitude and 24.5°N to 26°N latitude. The primary objective is to investigate the geochemical characteristics of cored sediments from the southwestern Okinawa Trough, in order to infer their source rocks and assess broader geological implications.

2. Analytical methods

Cored sediment samples for this study were collected using a piston corer deployed from the R/V Ocean Researcher I, operated by National Taiwan University. The sampling locations are shown in Fig. 1, and the coordinates along with basic metadata for each station are summarized in Table 1.

To ensure analytical representativity—particularly for trace elements present at parts-per-million (ppm; $\mu g \cdot g^{-1}$) levels—each sediment sample was processed from a minimum of 0.50000 g of dry material. In the laboratory, visually altered or discolored portions were removed using a water-cooled diamond saw. The remaining material was initially comminuted using a jaw crusher to <0.50 mm, homogenized, and then subdivided into aliquots of <50 g with a Retsch PT100 (SunPro International Inc., Taiwan) rotary splitter. These aliquots were further pulverized using a Siebtechnik (Mülheim an der Ruhr, Germany) vibratory puck-and-ring mill equipped with agate components to a grain size of <75 μm (200 mesh). Pulverized powders were homogenized and stored in sealed polyethylene (PE) vials. To prevent cross-contamination, all crushing and milling equipment was meticulously cleaned with quartzite and wiped with ethanol-moistened, lint-free paper between samples (Cox et al., 1995).

For mineralogical characterization, the clay fraction (<2 μm) was separated by gravitational sedimentation based on Stokes' Law, following dispersion with sodium hexametaphosphate and pH adjustment to ~9, as described by Jackson (1975) and Moore and Reynolds (1997). The separated clay was analyzed by X-ray diffraction (XRD) to identify dominant mineral phases.

Geochemical analyses of bulk sediments were conducted using multiple techniques. Major element oxides (SiO_2, Al_2O_3, TiO_2, and P_2O_5) were quantified using standard colorimetric procedures following acid digestion (Jeffery & Hutchison, 1981). The molybdenum blue method was applied for phosphorus (Murphy & Riley, 1962), and

Table 1

General description of the cores.

Station	Latitude	Longitude	Water depth (m)	Core recovery (cm)
2	24°56.2′N	122°51.6′E	1635	234
5	25°37′N	124°22′E	1900	230
11	25°11′N	124°00′E	2250	241
13	25°23′N	124°30′E	2050	215
15	25°38′N	125°00′E	2100	105

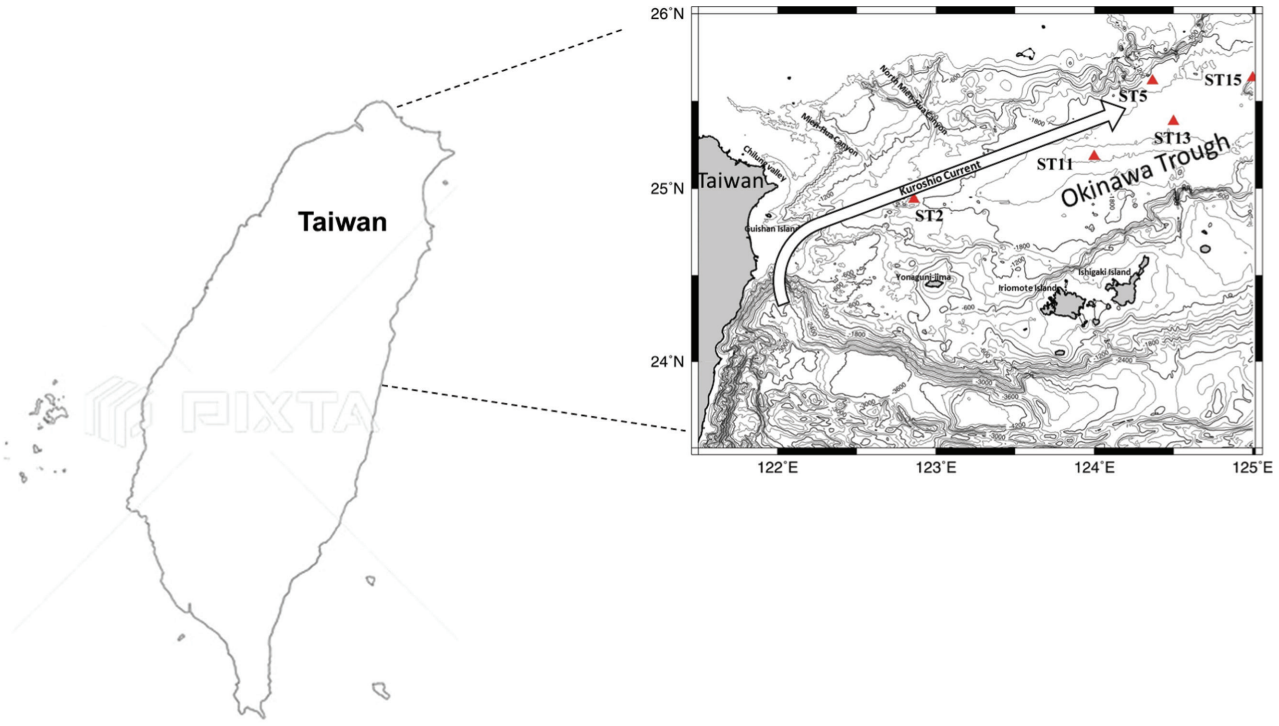

Figure 1

Location map shows the study area and the coring sites.

aluminon complexation was used for aluminum determination, with absorbance measured via Ultraviolet (UV)–Vis spectrophotometry. All measurements were performed in triplicate, and calibration curves were constructed using certified reference solutions.

Additional major elements (Fe, Mg, Ca, Na, K, and Mn) were determined by flame atomic absorption spectrometry (AAS) following standard protocols (PerkinElmer, 1996). Trace and rare earth elements (REEs) were analyzed using inductively coupled plasma mass spectrometry (ICP-MS) under optimized conditions to minimize spectral interferences, following methods outlined by Meisel et al. (1990) and Govindaraju (1989). Analytical accuracy and precision were evaluated using international geochemical reference materials United States Geological Survey (USGS) standards Hawaiian basalt reference material 1 (BHVO-1), Andesite reference material 1 (AGV-1), Basaltic andesite reference material 1 (BCR-1), W-2, G-2, and National Bureau of Standards (NBS) basalt standard), yielding uncertainties within ± 2% for major elements and ± 5% for trace and Rare Earth Elements (REEs).

The relative contributions of various source rocks to sediment composition can be estimated using a mixing model approach (Chen et al., 2017). By selecting appropriate end-member compositions—such as Graywack, shale, quartzite, and limestone—a computational model can be developed to quantify their respective inputs (Ho & Chen, 1996). This model operates under the following equation:

$$S = \alpha A + \beta B + gC + \delta D + \varepsilon$$

$$A = \sum_{j=1}^{n} W_{A(j)} \cdot X_j$$

$$B = \sum_{j=1}^{n} W_{B(j)} \cdot X_j$$

$$C = \sum_{j=1}^{n} W_{C(j)} \cdot X_j$$

$$D = \sum_{j=1}^{n} W_{D(j)} \cdot X_j$$

In this expression, *S* represents the elemental concentration in the sediment sample, while *A*, B, C, and D correspond to the elemental compositions of the selected end members. The coefficients α, β, γ, and δ indicate the proportional contribution of each end member, constrained to sum to unity. The term ε denotes the deviation between the modeled and observed values, which the model aims to minimize. *W* may be used to assign weights to specific elements, *j* denotes an individual chemical element, and *x* represents a variable in the model.

To simplify the modeling approach, it is assumed that the sediments reflect a single mixing event involving these three distinct end members. For each end member, the average values of major elemental compositions were used in the model to represent its characteristic geochemical signature. It is worth noting that the geochemical signature produced by a single mixing event may be similar to that generated through polycyclic sedimentary processes.

3. Results and discussion

3.1. Mineral compositions and chemical characteristics of cored sediments

XRD analysis of the core sediments reveals that the predominant clay minerals are illite, chlorite, and kaolinite, while the principal non-clay minerals include quartz, feldspar, calcite, and minor amounts of amphibole (Table 2). The results of major and trace element analyses for the cored sediments are presented in Tables 3–7. Major element compositions exhibit substantial variability across the different sampling stations. SiO_2 and Al_2O_3 are the most abundant oxides, jointly comprising approximately 63%–77% of the total sediment composition.

Manganese oxide (MnO), titanium dioxide (TiO_2), and phosphorus pentoxide (P_2O_5) occur in relatively low concentrations across all stations, while CaO and total iron (ΣFeO) are consistently higher than K_2O, MgO, and Na_2O. The concentrations of K_2O, MgO, and Na_2O are relatively uniform at stations ST2 and ST5, whereas more pronounced variability is observed at stations ST11, ST13, and ST15.

Among all cores, sediments from station ST13 display the highest average SiO_2 content, whereas their Al_2O_3 content is the lowest. This inverse relationship may reflect a relatively lower degree of chemical weathering. The lower Na_2O content compared to K_2O across the cores is interpreted as a result of the greater susceptibility of albite to chemical weathering relative to K-feldspar.

Fig. 2 presents the major element compositions of sediment cores from various stations, normalized to the Upper Continental Crust (UCC) values of Taylor and McLennan (1985). The results show that SiO_2 concentrations in all core samples are lower than the UCC reference. Notably, the decrease in SiO_2 content at Station ST15 is not accompanied by a corresponding increase in Al_2O_3, a pattern that may be linked to the elevated CaO content observed in these sediments.

Table 2

XRD results of core sediment samples (diffraction peak intensity in counts)

ST2						
Depth (cm)	Illite (8.9°)	Chlorite + Kaolinite (12.5°)	Quartz (20.9°)	Feldspar (27.8°)	Calcite (29.4°)	Amphibole (10.5°)
0	279	182	586	445	234	-
30	328	135	484	357	269	-
50	262	137	462	320	250	-
80	234	137	471	303	207	-
ST5						
Depth (cm)	Illite (8.9)	Chlorite + Kaolinite (12.5)	Quartz (20.9)	Feldspar (27.8)	Calcite (29.4)	Amphibole (10.5)
10	240	110	480	342	331	-
30	357	237	713	686	557	?
50	246	121	475	404	484	-
70	276	139	520	408	335	-
90	299	149	686	858	471	-
110	331	151	392	353	454	-
130	259	172	462	282	458	-
150	231	74	289	204	219	-
ST11						
Depth (cm)	Illite (8.9°)	Chlorite + Kaolinite (12.5°)	Quartz (20.9°)	Feldspar (27.8°)	Calcite (29.4°)	Amphibole (10.5°)
0–2.5	117	237	566	207	104	?
20–25	346	172	484	292	380	-
80–85	253	172	306	296	303	-
133–138	282	172	276	228	253	-
190–195	279	172	493	511	250	?
235–240	346	246	581	246	346	?
ST15						
Depth (cm)	Illite (8.9°)	Chlorite + Kaolinite (12.5°)	Quartz (20.9°)			
0–3	79	156	462			
8–14	234	121	467			
18–30	188	96	548			
44–46	296	98	400			
56–60	310	135	762			
100–105	259	177	339			
160–165	256	146	292			
213–215	172	98	424			
ST15						
Depth (cm)	Illite (8.9°)	Chlorite + Kaolinite (12.5°)	Quartz (20.9°)			
0–3	188	123	156			
7–11	346	190	376			
22–24	339	106	562			
45–50	339	40	207			
80–85	350	296	506			
100–105	339	117	424			

'?' indicates possible presence.
XRD, X-ray diffraction.

Table 3

Major and trace element compositions of cored sediments in the ST2 station of the SOT

Sample (cm)	0	30	50	80	Avg.
SiO_2 (wt%)	57.85	57.06	56.48	57.56	57.24
Al_2O_3	15.54	16.36	16.20	16.97	16.27
ΣFeO	6.65	6.77	6.63	6.44	6.62
MgO	3.43	3.51	3.50	3.53	3.49
CaO	2.18	2.52	2.75	2.78	2.56
Na_2O	1.38	1.45	1.36	1.35	1.39
K_2O	2.61	2.73	2.69	2.71	2.68
MnO	0.663	0.101	0.084	0.077	0.231
TiO_2	0.74	0.68	0.67	0.68	0.69
P_2O_5	0.16	0.13	0.12	0.12	0.13
LOI	8.89	8.69	9.09	9.00	8.92
Total	100.094	99.998	99.571	101.213	
Ba (ppm)	657	584	620	593	613
Co	14.8	14.0	14.2	14.0	14.3
Cr	90.6	85.7	90.0	85.2	87.9
Cu	56	35	34	34	40
Li	69.2	65.5	69.2	67.9	67.9
Nb	18.1	18.2	16.8	18.0	17.8
Ni	44.6	40.4	43.0	40.8	42.2
Rb	189	184	189	188	187
Sc	14.5	14.4	13.8	14.2	14.2
Sr	177	173	173	187	178
Ta	1.1	1.0	1.4	1.2	1.2
Th	12.2	9.7	11.0	11.3	11.1
U	2.06	1.81	1.84	1.91	1.91
V	140	134	129	127	133
Y	10.4	10.7	10.3	10.4	10.4
Zr	61	67	50	58	59
La	39.8	39.2	37.0	39.2	38.8
Ce	85.6	83.6	80.9	84.7	83.7
Nd	16.2	16.0	15.8	16.1	16.0
Sm	6.3	6.1	6.1	6.0	6.1
Eu	1.12	1.08	1.12	1.09	1.10
Gd	5.66	5.17	5.40	5.45	5.42
Tb	0.55	0.53	0.55	0.57	0.55
Yb	1.74	1.67	1.61	1.66	1.67
Lu	0.23	0.22	0.21	0.23	0.22

LOI, Loss on ignition; SOT, Southern Okinawa Trough.

Fig. 3 illustrates a positive correlation between ΣFeO and MgO with Al_2O_3, suggesting that the abundances of iron and magnesium are largely influenced by the presence of chlorite. Calcium, sodium, and potassium are primarily hosted in feldspar minerals. Variations in these elements across the cores likely reflect differences in source rock composition as well as the extent of chemical weathering. Although K_2O and Na_2O concentrations are relatively consistent across all cores, they are generally lower than UCC averages. This depletion may result from a reduced feldspar content in the source material or from feldspar breakdown during weathering.

Elevated CaO concentrations at Stations ST5, ST13, and ST15, relative to UCC values, are likely due to the presence of biogenic carbonate material (e.g., shell fragments) in some sediment layers. The relatively high MnO and ΣFeO contents at Station ST15 may reflect localized hydrothermal influence. TiO_2 concentrations are relatively uniform across all stations. Still, they are higher than UCC levels, possibly due to the relative immobility of Ti during weathering, allowing for its progressive enrichment in the residual sediment fraction.

Cox et al. (1995) introduced the index of compositional variability (ICV) as a means of evaluating the variability of aluminum relative to other major oxides in sedimentary rocks. The ICV is defined as:

$$ICV = (Fe_2O_3 + K_2O + Na_2O + CaO + MgO + MnO + TiO_2)/Al_2O_3$$

The ICV values of sediment cores analyzed in this study (Fig. 4) show notably higher variability at Stations ST13 and ST15, suggesting significant fluctuations in clay mineral content. Higher ICV values are typically indicative of a lower abundance of clay minerals and a greater proportion of non-clay detrital input.

Trace element concentrations of Co, Cr, Ni, V, and Sc are elevated in the ST2 core relative to other stations. These elements exhibit positive correlations with Al_2O_3, MgO, and total Fe (ΣFeO) (Figs. 5–7), suggesting that their distribution is closely associated with Fe–Mg-bearing minerals, particularly chlorite. A cross-plot of Cr/Th versus Sc/Th ratios in the sediment cores (Fig. 8) reveals a positive correlation, implying that the abundances of Cr, Sc, and Th are influenced by heavy mineral input and the presence of Fe–Mg-rich phases in the source rocks.

Data in Tables 3–7 indicate that Nb and Ta display relatively low mobility during weathering, whereas Th and U show broader compositional ranges, potentially reflecting differential geochemical behavior and partitioning during sedimentary differentiation and weathering processes.

Two samples—ST13 (44–46 cm) and ST15 (45–50 cm)—display elevated concentrations of Zr, Hf, and Y (Fig. 9), possibly indicating the presence of heavy minerals such as zircon. In contrast, cores from ST2 and ST5 exhibit higher Nb and Ta concentrations, which

Table 4

Major and trace element compositions of cored sediments in the ST5 station of the SOT

Sample (cm)	10	30	50	70	90	110	130	150	Avg.
SiO_2 (wt%)	59.27	57.56	57.35	55.98	56.94	55.90	55.48	56.48	56.87
Al_2O_3	15.34	15.13	14.78	14.42	14.67	14.42	14.67	14.77	14.78
ΣFeO	5.83	5.74	5.70	5.86	5.60	5.66	5.86	5.54	5.72
MgO	3.37	3.30	3.31	3.44	3.35	3.27	3.43	3.10	3.32
CaO	4.25	4.64	4.62	4.64	3.90	5.01	5.41	4.86	4.67
Na_2O	1.48	1.46	1.51	1.37	1.44	1.47	1.67	1.74	1.52
K_2O	2.44	2.20	2.21	2.24	2.44	2.43	2.60	2.31	2.36
MnO	0.062	0.069	0.081	0.085	0.075	0.066	0.085	0.082	0.076
TiO_2	0.62	0.67	0.64	0.64	0.58	0.71	0.61	0.55	0.63
P_2O_5	0.13	0.12	0.13	0.12	0.12	0.13	0.09	0.10	0.12
LOI	8.97	9.45	9.53	10.57	9.28	9.97	9.67	9.65	9.64
Total	101.765	100.342	99.858	99.361	98.397	99.039	99.574	99.186	
Ba (ppm)	566	567	549	512	546	544	423	479	523
Co	14.2	13.2	13.2	12.8	13.0	13.3	10.5	11.5	12.7
Cr	88.8	81.6	84.6	78.5	80.4	80.2	60.8	69.6	78.1
Cu	34	33	30	30	30	31	22	25	29
Li	68.2	65.3	65.3	65.2	28.8	63.0	47.9	54.4	57.3
Nb	15.8	16.5	17.5	17.1	17.3	15.8	10.5	11.6	15.3
Ni	47.5	39.2	38.9	37.8	38.6	41.1	29.2	33.8	38.3
Rb	170	166	163	163	166	165	119	136	156
Sc	13.6	12.6	12.8	12.6	13.5	13.2	8.9	11.0	12.3
Sr	224	253	254	254	224	252	175	209	231
Ta	0.9	1.2	1.0	1.0	1.0	0.9	0.8	0.9	1.0
Th	10.2	10.5	11.0	10.6	10.9	10.5	8.6	9.8	10.3
U	3.63	3.65	3.78	3.38	3.81	3.48	2.75	3.13	3.45
V	122	117	116	114	120	119	73	84	108
Y	10.8	10.7	10.9	10.7	10.9	10.7	9.8	10.4	10.6
Zr	62	67	79	75	74	61	53	64	67
La	37.4	39.4	41.7	37.5	39.2	38.0	28.8	31.3	36.7
Ce	79.2	82.7	87.1	79.5	83.4	80.9	61.7	68.0	77.8
Nd	16.1	16.4	16.7	15.6	16.3	16.0	13.2	14.3	15.6
Sm	6.1	6.4	6.4	5.9	6.2	6.1	5.0	5.6	6.0
Eu	1.10	1.12	1.11	1.02	1.07	1.06	0.87	0.98	1.04
Gd	5.52	5.71	5.95	5.46	5.70	5.26	4.49	5.28	5.42
Tb	0.56	0.57	0.62	0.57	0.59	0.56	0.47	0.57	0.56
Yb	1.68	1.74	1.77	1.73	1.76	1.72	1.65	1.99	1.76
Lu	0.21	0.23	0.23	0.23	0.24	0.22	0.24	0.29	0.24

LOI, Loss on ignition; SOT, Southern Okinawa Trough.

may reflect input from accessory phases such as rutile or ilmenite.

Fig. 10 illustrates the relationship between REE concentrations and Al_2O_3 in the sediment cores. A general positive correlation suggests that REEs are likely adsorbed to clay minerals, which serve as key carriers during sediment transport and deposition.

Fig. 11 shows chondrite-normalized REE patterns for samples with the highest and lowest REE concentrations in this study, alongside reference

Table 5

Major and trace element compositions of cored sediments in the ST11 station of the SOT

Sample (cm)	0–2.5	20–25	80–85	133–138	190–195	235–240	Avg.
SiO_2 (wt%)	59.10	55.16	55.10	55.89	62.73	67.10	59.18
Al_2O_3	14.27	13.91	14.52	13.76	11.82	9.06	12.89
ΣFeO	8.76	6.67	7.14	7.04	5.70	3.93	6.54
MgO	2.98	4.04	3.78	3.83	3.45	2.65	3.46
CaO	3.37	2.73	2.67	2.70	3.12	5.39	3.33
Na_2O	1.48	1.21	1.13	1.24	1.59	1.76	1.40
K_2O	1.89	2.94	2.77	3.02	2.44	1.92	2.50
MnO	0.239	0.165	0.142	0.134	0.111	0.081	0.145
TiO_2	0.72	0.72	0.69	0.69	0.65	0.54	0.67
P_2O_5	0.13	0.11	0.09	0.12	0.12	0.11	0.11
LOI	8.72	11.5	11.4	10.87	8.18	6.96	9.61
Total	101.656	99.157	99.436	99.292	99.908	99.499	
Ba (ppm)	469	516	429	528	466	401	468
Co	14.7	15.2	12.6	13.9	12.5	11.0	13.3
Cr	80.4	95.4	82.8	90.4	76.6	62.7	81.4
Cu	53	40	32	35	27	16	34
Li	48.2	77.5	64.4	74.9	59.8	36.8	60.3
Nb	11.5	14.0	11.6	13.3	12.7	10.8	12.3
Ni	41.3	44.7	39.5	42.1	35.9	31.5	39.1
Rb	132	184	151	178	145	101	149
Sc	9.4	14.0	11.6	13.1	11.4	7.9	11.2
Sr	165	154	126	153	147	180	154
Ta	0.8	0.9	0.7	1.1	0.9	0.8	0.9
Th	7.7	9.9	8.2	11.4	7.8	7.7	8.8
U	1.46	2.28	1.77	2.37	1.71	1.71	1.88
V	90	123	103	117	99	64	99
Y	9.8	10.3	9.8	10.1	9.9	9.6	9.9
Zr	43	57	48	51	46	42	48
La	31.5	34.4	28.6	33.4	32.0	30.3	31.7
Ce	65.6	73.3	61.2	73.0	69.6	64.2	67.8
Nd	14.0	14.9	12.6	15.0	14.7	14.1	14.2
Sm	5.3	5.6	4.7	5.8	5.6	5.3	5.4
Eu	0.95	0.99	0.81	1.03	0.98	0.91	0.95
Gd	4.64	4.95	4.03	5.52	4.84	5.17	4.86
Tb	0.47	0.49	0.41	0.55	0.49	0.49	0.48
Yb	1.50	1.68	1.42	1.68	1.46	1.38	1.52
Lu	0.20	0.23	0.19	0.25	0.20	0.21	0.21

LOI, Loss on ignition; SOT, Southern Okinawa Trough.

values for shale, quartzite, and the UCC. The REE concentrations of the cored sediments lie between those of shale and quartzite, with a modest enrichment in light REEs (LREEs) and a pronounced negative europium (Eu) anomaly. This REE signature is broadly consistent with that of the UCC and may reflect the removal or alteration of plagioclase during weathering or diagenesis.

The geochemical behavior of REEs in marine sediments is closely linked to their interaction

Table 6

Major and trace element compositions of cored sediments in the ST13 station of the SOT

Sample (cm)	0–3	8–14	18–30	44–46	56–60	100–105	160–165	213–215	Avg.
SiO_2 (wt%)	56.44	59.89	69.19	70.48	63.60	60.62	56.48	59.98	62.09
Al_2O_3	7.17	11.20	8.43	11.00	9.47	11.56	14.83	12.94	10.83
ΣFeO	3.77	6.51	4.37	3.34	3.87	6.71	7.01	5.97	5.19
MgO	2.40	3.52	2.57	1.21	2.58	3.85	3.98	3.50	2.95
CaO	14.78	3.98	4.24	2.91	6.93	2.24	2.16	3.06	5.04
Na_2O	1.68	1.43	1.88	3.11	1.68	1.36	1.26	1.47	1.73
K_2O	1.46	2.43	1.63	2.10	1.80	3.06	2.85	2.34	2.21
MnO	0.112	0.079	0.073	0.121	0.058	0.100	0.100	0.110	0.094
TiO_2	0.45	0.64	0.87	0.52	0.57	0.63	0.58	0.62	0.61
P_2O_5	0.10	0.10	0.15	0.08	0.11	0.10	0.09	0.10	0.10
LOI	11.28	10.66	6.10	5.59	9.16	9.30	10.06	9.41	8.95
Total	99.640	100.440	99.499	100.456	99.827	99.534	99.402	99.495	
Ba (ppm)	386	485	380	415	406	462	424	434	424
Co	12.4	12.0	9.2	6.5	10.9	13.8	13.2	12.0	11.2
Cr	47.9	76.3	57.9	16.5	49.8	84.8	78.4	70.8	60.3
Cu	15	30	17	11	12	27	27	23	20
Li	33.2	61.2	32.8	26.2	39.0	76.8	75.9	63.9	51.1
Nb	10.1	12.7	14.4	6.9	11.0	12.1	9.7	12.2	11.1
Ni	31.0	39.2	23.9	13.2	26.0	37.9	37.3	33.2	30.2
Rb	89	154	95	88	104	166	163	143	125
Sc	6.7	11.2	8.4	8.6	7.9	14.7	11.8	11.1	10.1
Sr	356	198	171	163	239	118	97	139	185
Ta	0.7	0.8	1.0	0.4	0.7	0.8	0.6	0.8	0.7
Th	5.7	8.9	9.8	6.1	7.2	10.3	8.1	9.5	8.2
U	1.54	1.78	1.95	2.00	1.82	2.17	1.78	2.13	1.90
V	57	102	67	41	68	107	98	90	79
Y	9.3	9.9	10.5	11.8	9.7	10.0	9.7	9.8	10.1
Zr	42	52	61	106	47	49	38	48	55
La	23.8	29.6	48.9	19.9	27.9	30.5	27.8	30.8	29.9
Ce	51.2	65.5	102.9	46.1	59.4	68.0	62.2	68.4	65.5
Nd	11.4	13.8	20.9	11.1	12.9	14.4	13.1	14.3	14.0
Sm	4.1	5.2	8.1	4.7	4.8	5.7	5.0	5.3	5.4
Eu	0.79	0.98	1.20	0.89	0.87	0.98	0.91	1.02	0.96
Gd	4.20	4.93	7.18	4.59	5.00	5.60	4.56	5.27	5.17
Tb	0.44	0.50	0.67	0.59	0.49	0.54	0.45	0.53	0.53
Yb	1.25	1.55	1.71	2.56	1.43	1.53	1.41	1.62	1.64
Lu	0.19	0.22	0.24	0.39	0.21	0.23	0.18	0.23	0.24

LOI, Loss on ignition; SOT, Southern Okinawa Trough.

with fine-grained mineral phases, particularly clay minerals. In the present study, REE concentrations were found to exhibit a positive correlation with Al_2O_3 and other clay-associated elements, suggesting a key role for clay minerals in REE retention. This observation is consistent with recent findings by Cai et al. (2023), who demonstrated a significant positive correlation between total REY concentrations and clay mineral content in deep-sea sediments. Their study emphasized that kaolinite, in particular, acts as

Table 7

Major and trace element compositions of cored sediments in the ST15 station of the SOT

Sample (cm)	0–3	7–11	22–24	45–50	80–85	100–105	Avg.
SiO_2 (wt%)	54.44	49.65	50.19	65.56	54.94	51.48	54.38
Al_2O_3	13.65	13.50	8.40	12.22	14.11	14.06	12.66
ΣFeO	10.74	11.00	9.19	3.90	6.80	8.24	8.31
MgO	3.73	3.45	2.43	1.52	3.93	3.89	3.16
CaO	3.19	4.88	14.12	3.30	3.34	4.39	5.54
Na_2O	1.34	1.35	1.50	3.11	1.39	1.27	1.66
K_2O	2.58	2.40	1.39	2.65	3.04	2.90	2.49
MnO	0.924	0.822	0.105	0.102	0.118	0.244	0.386
TiO_2	0.71	0.77	0.51	0.58	0.67	0.62	0.64
P_2O_5	0.13	0.15	0.09	0.09	0.12	0.11	0.12
LOI	8.85	11.78	12.59	7.06	10.41	12.71	10.57
Total	100.288	99.748	100.513	100.094	98.869	99.909	
Ba (ppm)	502	483	275	395	471	495	437
Co	15.9	16.4	12.7	5.9	13.9	15.5	13.4
Cr	88.5	80.5	58.2	16.8	79.8	101.0	70.8
Cu	58	67	41	15	31	44	42.7
Li	57.4	51.3	27.7	32.4	70.8	72.1	52.0
Nb	10.9	9.8	9.2	7.0	12.6	11.7	10.2
Ni	48.3	53.5	34.5	12.5	42.1	54.8	40.9
Rb	141	126	71	95	158	161	125
Sc	10.8	10.1	6.1	10.2	12.2	7.9	9.5
Sr	160	191	327	185	168	220	208
Ta	0.7	0.6	0.6	0.4	0.7	0.7	0.6
Th	7.9	7.2	5.6	5.9	9.5	8.3	7.4
U	1.51	1.30	1.63	2.22	2.22	1.95	1.81
V	100	98	52	47	107	113	86
Y	9.5	9.5	9.2	12.0	9.8	9.8	9.9
Zr	38	38	44	117	49	47	55.5
La	25.7	24.8	22.2	18.4	29.7	27.9	24.8
Ce	56.1	52.0	47.6	42.5	62.0	61.3	53.6
Nd	12.2	11.4	10.5	10.4	13.4	12.9	11.8
Sm	4.5	4.2	3.7	4.4	5.1	4.8	4.4
Eu	0.84	0.75	0.64	0.84	0.92	0.92	0.82
Gd	4.35	3.96	3.98	4.45	5.14	4.85	4.46
Tb	0.42	0.39	0.39	0.58	0.52	0.46	0.46
Yb	1.38	1.28	1.19	2.73	1.50	1.45	1.59
Lu	0.19	0.17	0.16	0.40	0.21	0.20	0.22

LOI, Loss on ignition; SOT, Southern Okinawa Trough.

a major carrier of REYs, and that clay minerals—rather than only Fe–Mn oxides or biogenic apatite—play an active role in REY accumulation through surface adsorption and mineral–water interactions near the sediment-water interface.

Furthermore, Dou et al. (2010) analyzed the temporal evolution of clay mineral assemblages in the central Okinawa Trough over the last 28 ka, showing that variations in illite, smectite, and kaolinite abundances reflect changes in terrigenous input, driven primarily

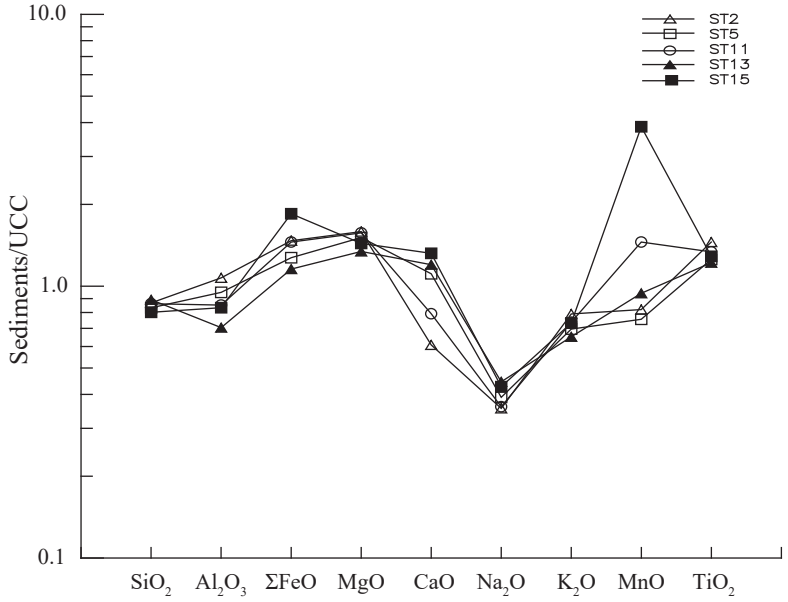

Figure 2

UCC (Taylor & McLennan, 1985) normalized major element variations for cored sediments of this study. UCC, Upper continental crust.

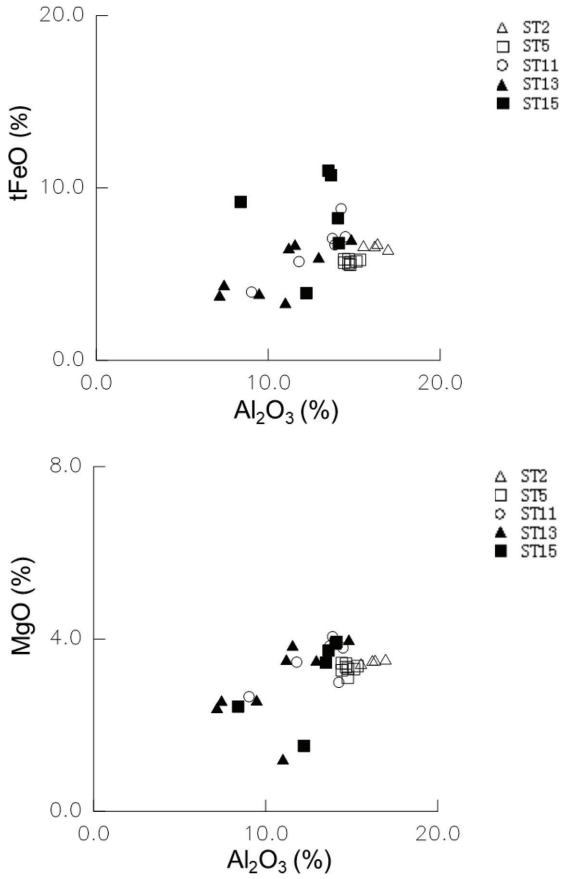

Figure 3

Al_2O_3 versus ΣFeO and MgO plots for cored sediments of this study.

by the East Asian monsoon and shifts in fluvial sources. While their study did not directly analyze REEs, the compositional variability of clay minerals suggests that source-related changes could significantly influence the REE adsorption capacity and fractionation patterns, especially along vertical sediment profiles.

In addition, sediment transport time and depositional dynamics also affect the availability and binding of REEs to clay particles. Li et al. (2016) used Nd isotope systematics to constrain the timescales of lithogenic sediment transport from the Yangtze River to the Okinawa Trough, revealing that fine-grained particles (including clays) undergo delayed deposition due to extended transport distances. This prolonged residence time potentially enhances the opportunity for REEs to be adsorbed onto clay surfaces during suspension in seawater.

Taken together, these findings support the interpretation that REE enrichment in the studied sediments results from a combination of clay mineral abundance, compositional variation related to sediment provenance, and prolonged particle–seawater interaction during sediment transport. Therefore, the spatial and vertical variability of REE concentrations in the core sediments may reflect both mineralogical control and dynamic depositional conditions in the Okinawa Trough.

3.2. Contributions of different source rocks

Owing to its geographical location, geomorphological setting, and prevailing

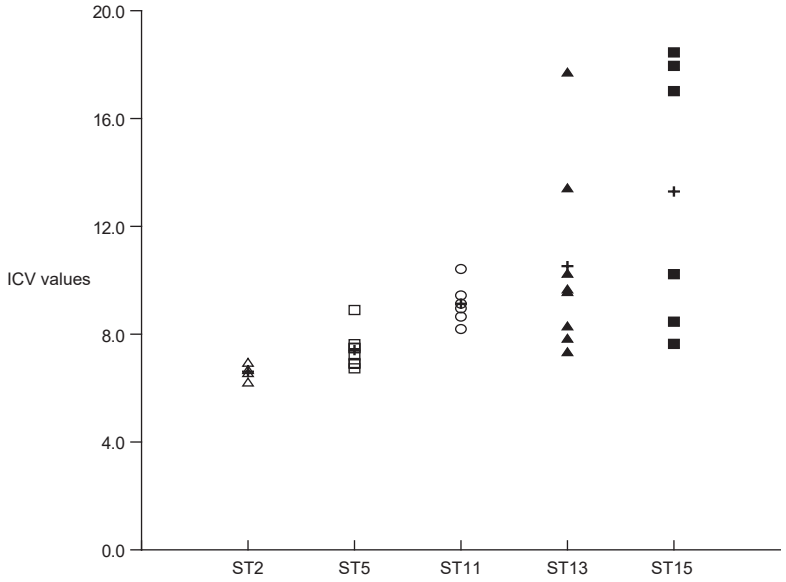

Figure 4

ICV values of the sediment cores in this study (+: the mean values of ICV for each station). ICV, Index of compositional variability.

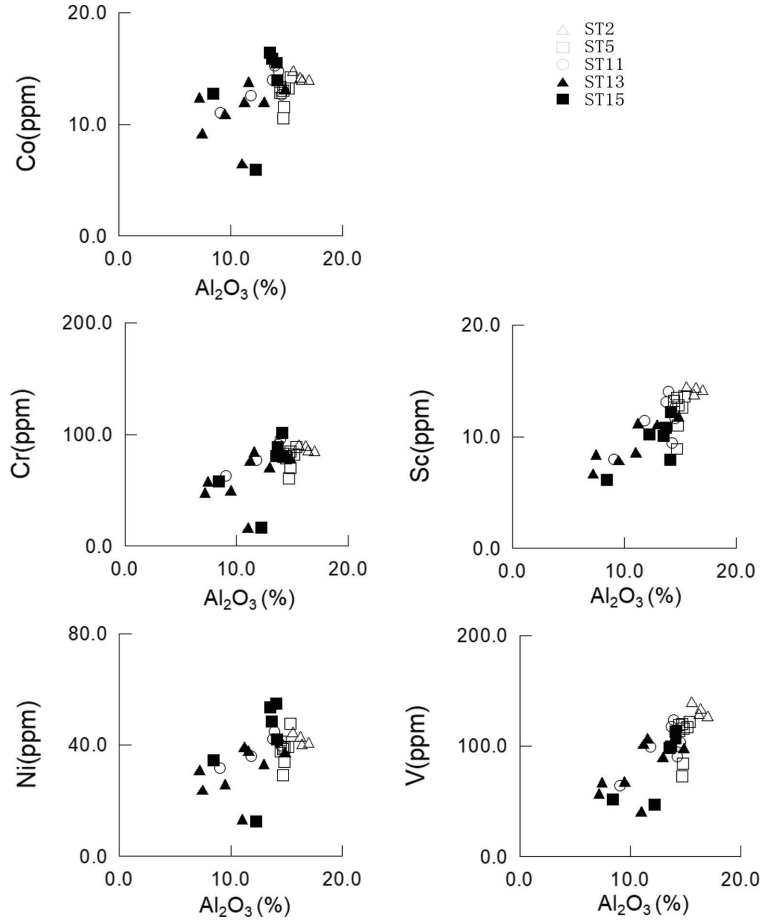

Figure 5

High field strength elements versus Al_2O_3 plots for cored sediments in this study.

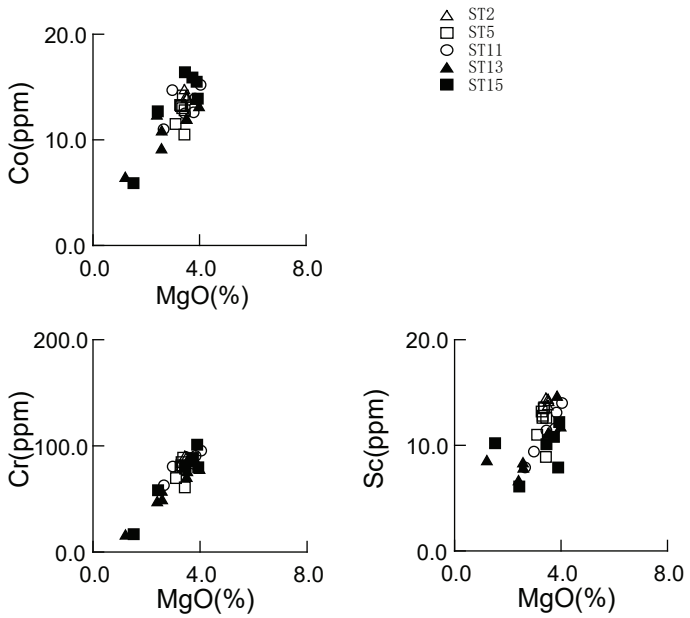

Figure 6

High field strength elements versus MgO plots for cored sediments in this study.

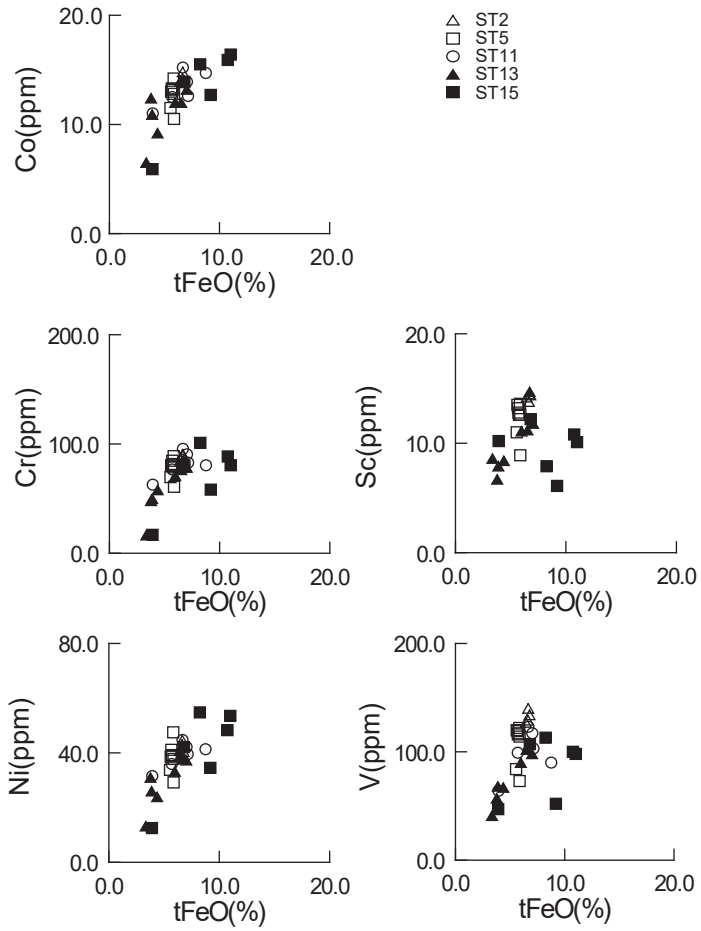

Figure 7

High field strength elements versus ΣFeO plots for cored sediments of this study.

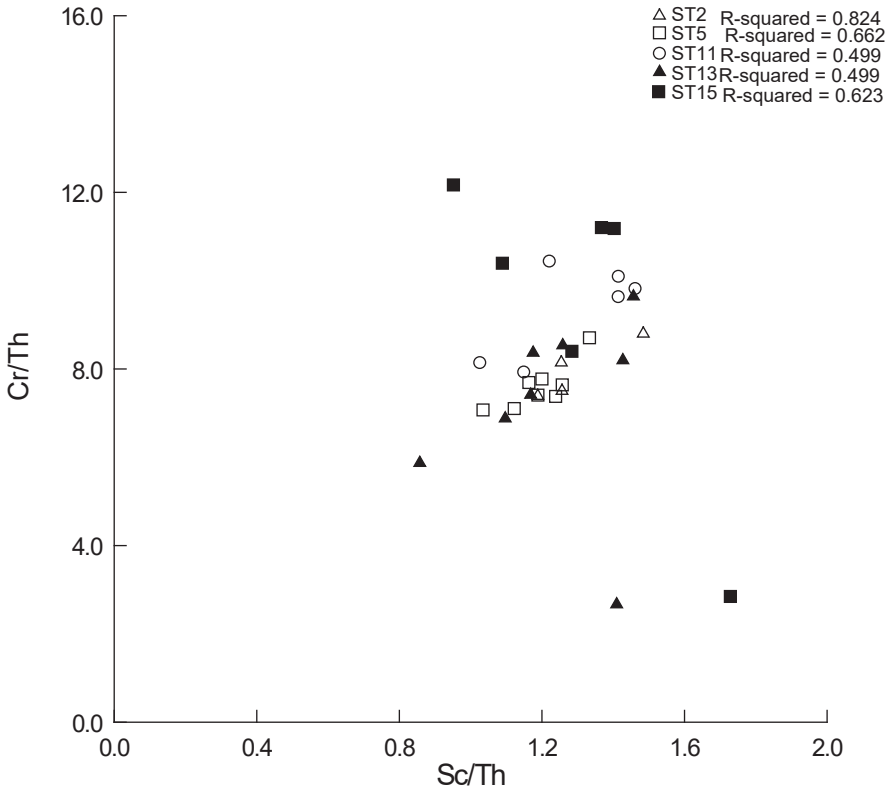

Figure 8

Cr/Th versus Sc/Th plots for the cored sediments of this study.

hydrodynamic conditions, the southernmost segment of the SOT serves as an efficient sediment sink, receiving input from both Taiwan and the East China Sea continental shelf (Lee et al., 2004). Geochemically stable elements such as REEs, Th, Sc, and Co are resistant to alteration during weathering, transport, diagenesis, and metamorphism, and are therefore commonly employed as proxies for determining sediment provenance. The La–Th–Sc ternary diagram is particularly useful for discriminating between felsic and mafic source rocks (Cullers, 1994; Nyakairu & Koeberl, 2001).

As shown in Fig. 12, the sediment samples analyzed in this study plot within the compositional field representative of mixed sources—including clay, silt, sand, and gravel—similar to sediments offshore northern Taiwan (Chao & Chen, 2003). Roser and Korsch (1986) proposed a classification scheme based on major element geochemistry, delineating four provenance types: felsic igneous, quartzose sedimentary, mafic igneous, and intermediate igneous sources. In Fig. 13, the REE distribution patterns and associated trace element signatures suggest that a portion of the sediment material is indeed derived from the weathering of volcanic rocks on Guishan Island, as evidenced by enrichment in LREEs and elevated Th and La concentrations. However, a more comprehensive interpretation must also consider the multi-source nature of the sediments and the influence of post-depositional processes. The normalized REE patterns indicate not only a volcanic contribution but also the presence of terrigenous detritus, likely sourced from the Lan-Yang River and the East China Sea continental shelf, as supported by the three-end-member mixing model results. Samples showing relatively flat REE patterns with slight Eu anomalies could be indicative of sediment mixing between felsic continental sources and local mafic volcanic input. Additionally, variations in $(La/Yb)_N$ and $(Gd/Yb)_N$ ratios among the samples suggest differential sediment contribution from sources with contrasting degrees of weathering and sorting during transport. It is also important to recognize that REE mobility can be influenced by sedimentary redox conditions, grain size sorting, and clay mineral associations. The positive correlation between REEs and Al_2O_3 in the same samples, as discussed earlier, further implies that fine-grained clay minerals serve as major carriers of REEs and that authigenic or diagenetic processes may have modified the primary geochemical

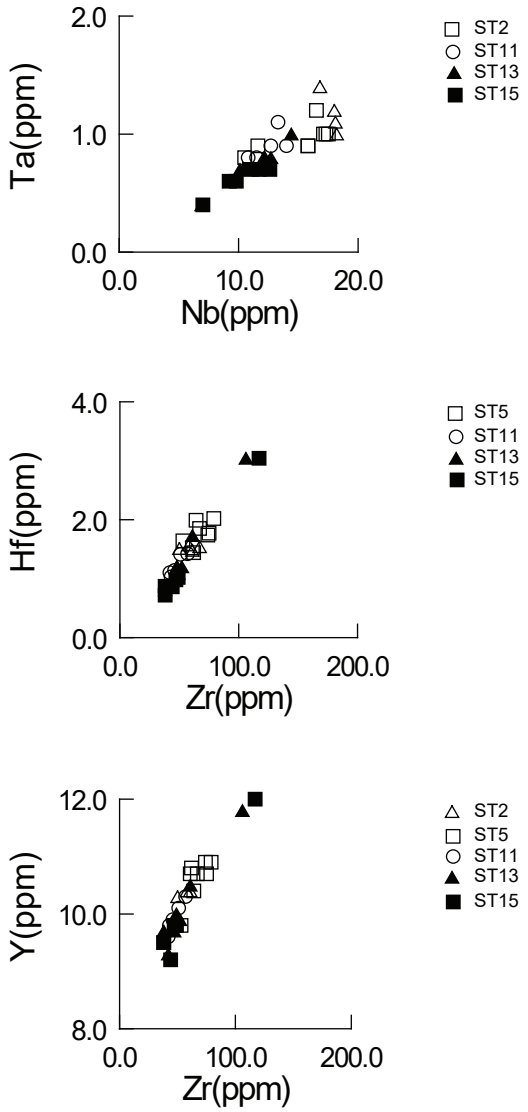

Figure 9

Nb versus Ta and Zr versus Hf, Y plots for cored sediments of this study.

signature. Taken together, the patterns presented in Fig. 13 should be interpreted not solely as evidence of Guishan volcanic input, but as the integrated result of multi-source sediment supply, mechanical sorting during transport, chemical weathering intensity, and early diagenetic overprinting under varying bottom-water conditions in the Okinawa Trough.

$$DF1 = -1.773\ TiO_2 + 0.607\ Al_2O_3 + 0.76\ tFeO - 1.5\ MgO + 0.616CaO + 0.509\ Na_2O - 1.224\ K_2O - 9.09$$

$$DF2 = 0.445\ TiO_2 + 0.07\ Al_2O_3 - 0.25\ tFeO - 1.142\ MgO + 0.438\ CaO + 0.475\ Na_2O + 1.426\ K_2O - 6.861$$

Fig. 14 illustrates that most of the cored sediments from this study are situated within the active continental margin field, supporting the interpretation that the SOT is currently undergoing early-stage back-arc extension.

The La–Th–Sc plots (Fig. 12) indicate that the cored sediments analyzed in this study are derived from mixed provenance sources. Based on the geochemical signatures of these sediments, three end-member compositions were selected for provenance modeling: (1) cored sediments from the Lan-Yang area in northeastern Taiwan, (2) sediments from the East China Sea continental shelf, and (3) volcanic rocks from the Okinawa Trough, as reported in previous studies (Chen & Kato, 1989; Chen & Lin, 1994; Lee, 2002; Table 7). These end members were incorporated into a three-component mixing model developed by Ho and Chen (1996) to estimate the relative contributions from each source.

To simplify the modeling approach, it is assumed that the sediments reflect a single mixing event involving these three distinct end members. It is worth noting that the geochemical signature produced by a single mixing event may be similar to that generated through polycyclic sedimentary processes. The model results are presented in Table 8. According to the calculations, the dominant source of sediments is the Lan-Yang area (averaging 54.63%), followed by the East China Sea continental shelf (24.12%) and volcanic input from the Okinawa Trough (21.25%). These results support the interpretation that fluvial input from Taiwan and sediment from the East China Sea shelf represent the primary sources for sediment accumulation in the SOT.

Li et al. (2009) proposed that the Lan-Yang River in northeastern Taiwan is a major sediment contributor, transporting approximately 10 million metric tons of material annually to the adjacent coastal and offshore regions. Some of this material is likely transported northward by ocean currents into the southwestern Okinawa Trough. Huh et al. (2006) noted that sedimentation rates in the SOT generally decrease with increasing water depth and distance from the coastline, except in localized bathymetric depressions below the 1400 m isobath, where episodic turbidite deposition enhances sediment accumulation. The principal supply of detrital sediment to the region is derived from fluvial runoff originating in Taiwan's central mountain ranges, driven by steep topographic gradients and intense monsoonal rainfall (Hsu et al., 2004). In northern Taiwan, sediment discharge is primarily funneled through the Lan-Yang River, which debouches into the sea adjacent to the SOT.

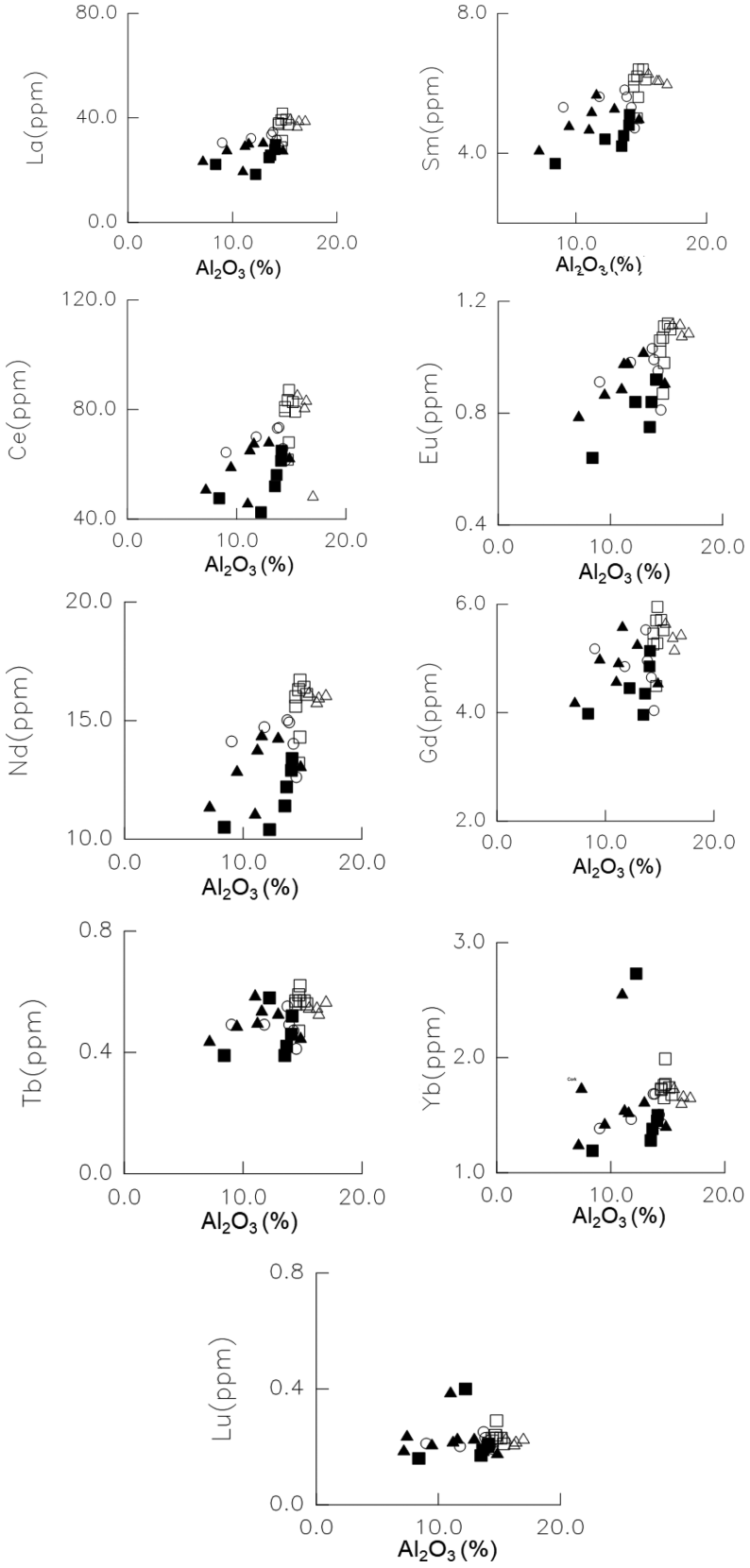

Figure 10

REEs versus Al_2O_3 plots for cored sediments of this study. REEs, rare earth elements.

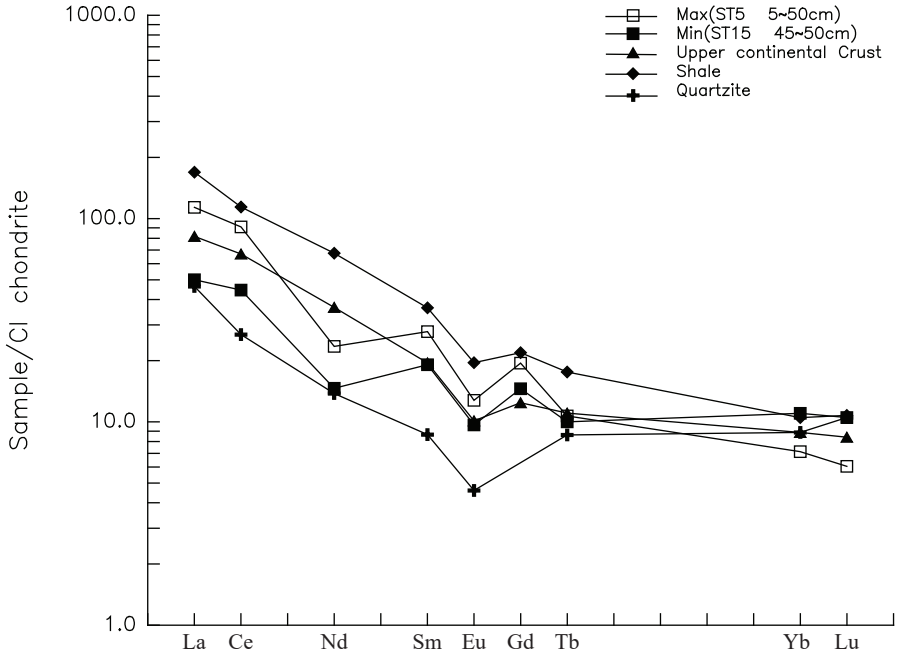

Figure 11

Range of chondrite-normalized REE patterns for cored sediments in this study as compared with shale, quartzite, and UCC. Shale from Govindaraju (1989). Quartzite from Meisel et al. (1990). Upper continental crust from Taylor and McLennan (1985). REE, rare earth element; UCC, upper continental crust.

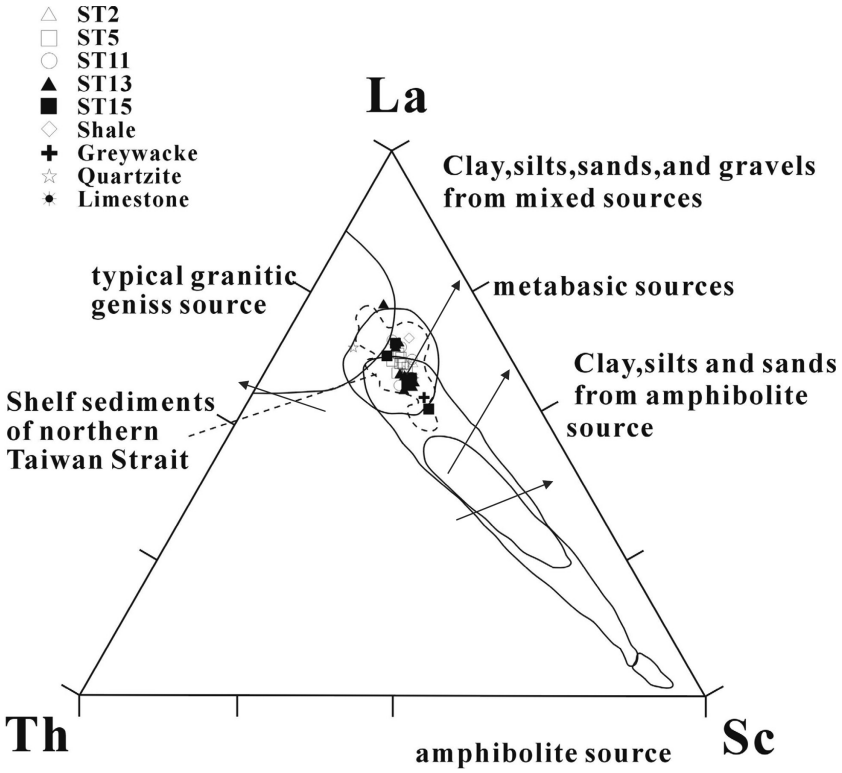

Figure 12

La–Th–Sc variations for cored sediments (variation fields modified from Cullers, 1994). Shale and limestone from Govindaraju (1989). Greywacke from Condie (1993). Quartzite from Meisel et al. (1990).

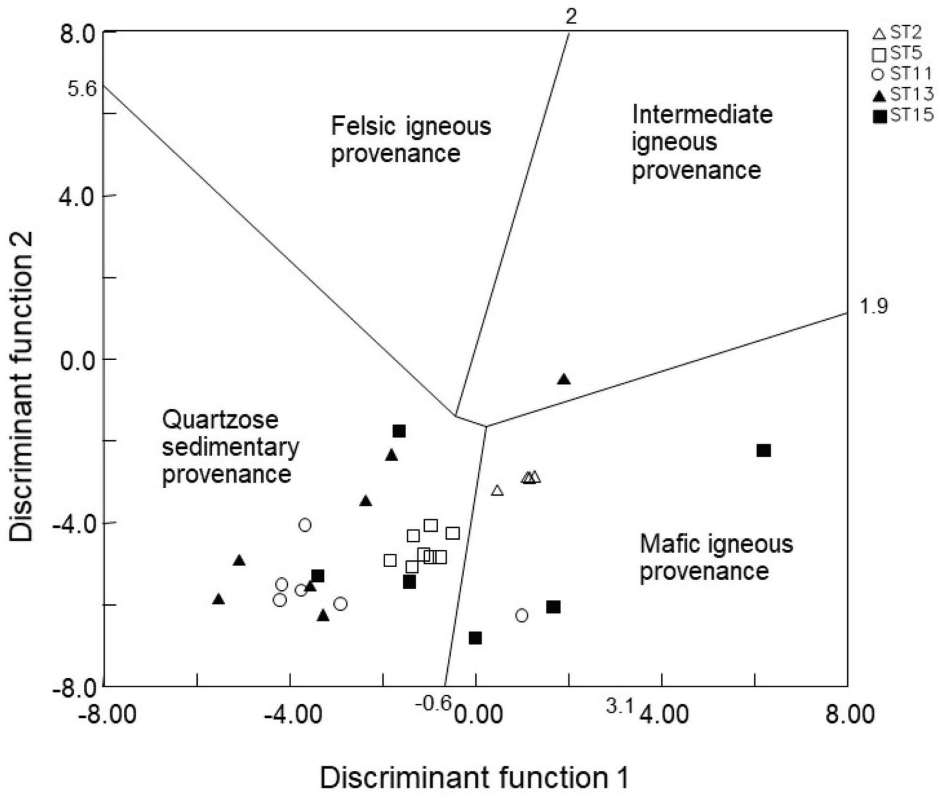

Figure 13

DF1 versus DF2 plots for cored sediments in this study (variation fields modified from Roser & Korsch, 1986).

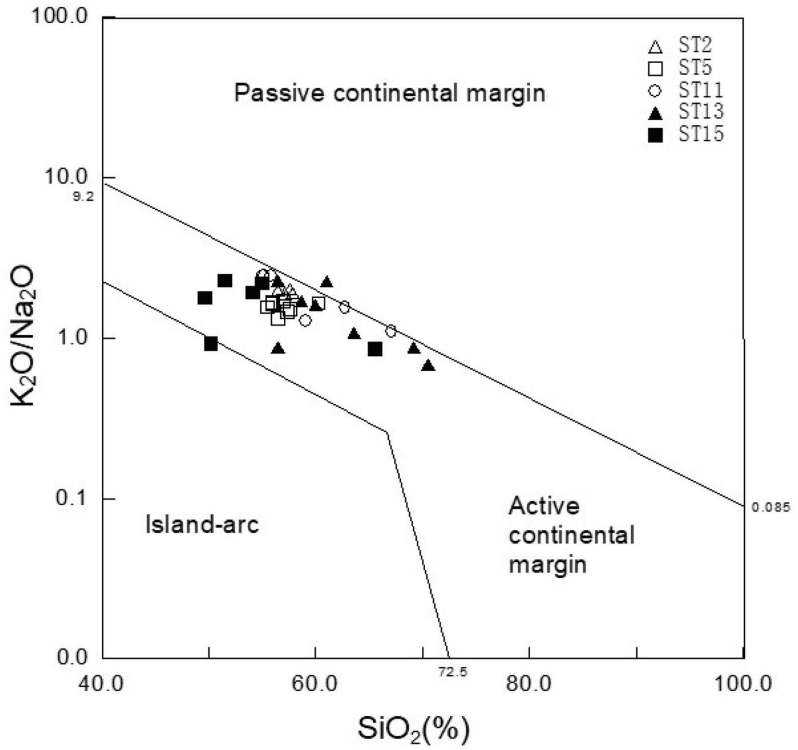

Figure 14

K_2O/Na_2O versus SiO_2 plots for cored sediments in this study (variation fields modified from Roser & Korsch, 1986).

Table 8

Chemical compositions of the cored sediments, end members, and results of mixing model calculations

	1	2	3	4	5	6	7	8	9
	ST2	ST5	ST11	ST13	ST15	ST5.11. 13.15 (Average)	Average of cored sediments from the Lan-Yang area (EM1)	Average of sediments from the East China Sea continental shelf (EM2)	Average of the Okinawa Trough volcanic rocks (EM3)
(wt%)									
SiO_2	57.24	56.87	59.18	62.09	54.38	58.13	62.65	59.87	52.67
Al_2O_3	16.27	14.78	12.89	10.83	12.66	12.79	16.96	8.62	17.70
ΣFeO	6.62	5.72	6.54	5.19	8.31	6.44	7.02	3.88	8.04
MgO	3.5	3.32	3.45	2.95	3.16	3.22	1.70	1.67	3.87
CaO	2.56	4.67	3.33	5.04	5.54	4.65	0.93	10.75	9.30
Na_2O	1.39	1.52	1.40	1.73	1.66	1.58	0.82	1.12	3.24
K_2O	2.68	2.36	2.50	2.21	2.49	2.39	3.02	2.06	1.15
MnO	0.23	0.08	0.15	0.09	0.39	0.18	0.08	0.16	0.15
Results of the mixing model calculations									
	ST2	ST5	ST11	ST13	ST15				
EM1	71.22%	52.93%	65.72%	47.56%	35.73%	51.88%			
EM2	0.00%	18.50%	27.51%	52.44%	22.15%	31.80%			
EM3	28.78%	28.57%	6.76%	0.00%	42.12%	16.33%	□	□	□

1–6: This study.
7: Average of cored sediments from the Lan-Yang area (Lee, 2002).
8: Average of sediments from the East China Sea continental shelf (Chen & Lin, 1994).
9: Average of the Okinawa Trough volcanic rocks (Chen & Kato, 1989).

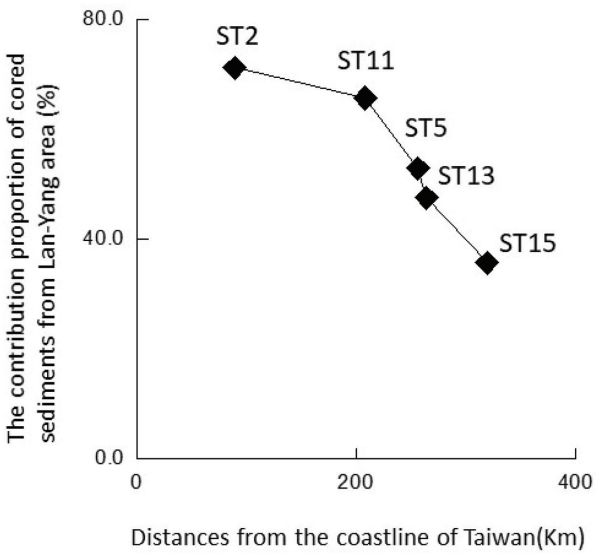

Figure 15

Variation diagram of the contribution proportion of core sediments from the Lan-Yang area at distances from the coastline of Taiwan.

Detrital zircon U–Pb geochronology from Zhu and Zeng (2022) confirms that over the past 700 years, sediment accumulation in the SOT reflects contributions from Taiwanese rivers, the East China Sea shelf, and the Yangtze River. In the present study, the proportion of Lan-Yang-derived material in the sediment cores generally decreases with increasing distance from the northeastern Taiwan coastline (Fig. 15).

4. Conclusions

The cored sediments analyzed in this study are primarily composed of quartz, feldspar, illite, chlorite + kaolinite, and calcite, with minor amounts of hornblende. Based on the positive correlation observed between REE concentrations and Al_2O_3 content, it is inferred that clay mineral adsorption plays a significant role in controlling REE distribution within the sediments. A plot of $\log(K_2O/Na_2O)$ versus SiO_2 indicates that the majority of samples fall within the active continental margin field, supporting the interpretation that the SOT is currently in an early stage of extensional tectonics.

The chondrite-normalized REE patterns exhibit a negative europium (Eu) anomaly, which may reflect the removal or alteration of plagioclase during weathering or diagenetic processes. La–Th–Sc ternary plots further suggest that the sediments are derived from mixed provenance sources.

Provenance modeling, based on the mixing model of Ho and Chen (1996), reveals that the primary contributor to the cored sediments is the Lan-Yang area in northeastern Taiwan, accounting for an average of 54.63%, followed by sediments from the East China Sea continental shelf (24.12%) and volcanic material from the Okinawa Trough (21.25%). These results indicate that fluvial input from Taiwan and sediment transported from the East China Sea shelf are the dominant sources for sedimentation in the SOT.

Acknowledgments

We would like to thank Professor J. C. Chen from the Institute of Oceanography at National Taiwan University for providing the cored sediment for this research.

Author contributions

Conceptualization, Y.T. Lee; methodology, Y.T. Lee; writing—original draft preparation, Y.T. Lee, I-An Chang, Huang, Ren-Yi, and M. L. Lin; writing—review and editing, Y.T. Lee, I-An Chang, Huang, Ren-Yi, and M. L. Lin. All authors have read and agreed to the published version of the manuscript.

References

Cai, Y.-C., Shi, X., Zhou, T., Huang, M., Yu, M., Zhang, Y., Bi, D., Zhu, A., & Fang, X. (2023). Evaluating the contribution of hydrothermal fluids and clay minerals to the enrichment of rare earth elements and yttrium (REY) in deep-sea sediments. *Ore Geology Reviews, 161*, 105679. https://doi.org/10.1016/j.oregeorev.2023.105679

Chao, H. J., & Chen, J. C. (2003). Grain size, mineralogical and chemical characteristics of cored sediments from offshore Hsinchu and their geological implications. *Acta Oceanographica Taiwanica, 41*(1), 61–96.

Chen, H. Y., Ikuta, R., Lin, C. H., Hsu, Y. J., Kohmi, T., Wang, C. C., Yu, S. B., Tu, Y., Tsujii, T., & Ando, M. (2017). Back-arc opening in the western end of the Okinawa Trough revealed from GNSS/acoustic measurements. *Geophysical Research Letters, 45*(1), 137–145. https://doi.org/10.1002/2017GL075724

Chen, J. C., & Kato Y. (1989). Geochemistry of volcanic rocks from the Ryukyu Islands: Compared with andesitic rocks from northern Taiwan. *Acta Oceanographica Taiwanica, 22*, 116–128.

Chen, J. C., & Lin, F. J. (1994). Survey and analysis of coastal marine sand distribution and composition in northern Taiwan. (pp. 1–126). Research Report Commissioned by the Central Geological Survey, Ministry of Economic Affairs.

Chen, M. P., & Kuo, C. L. (1980). Grain size analysis of the sediments of the southern Okinawa Trough. *Proceedings of the Geological Society of China, 23*, 105–117.

Chung, Y. C., & Hung, G. W. (2000). Particulate fluxes and transports on the slope between the southern East China Sea and the South Okinawa Trough. *Continental Shelf Research, 20*, 571–597. https://doi.org/10.1016/S0278-4343(99)00086-2

Condie, K. C. (1993). Chemical composition and evolution of the upper continental crust: Contrasting results from surface samples and shales. *Chemical Geology, 104*(1-4), 1–37. https://doi.org/10.1016/0009-2541(93)90140-E

Cox, R., Lowe, D. R., & Cullers, R. L. (1995). The influence of sediment recycling and basement composition on evolution of mudrock chemistry in the southwestern United States. *Geochimica et Cosmochimica Acta, 59*(14), 2919–2940. https://doi.org/10.1016/0016-7037(95)00185-9

Cullers, R. L. (1994). The controls on the major and trace elements variation of shales, siltstones and sandstones of Pennsylvanian-Permian age from uplifted continental blocks in Colorado to platform sediments in Kansas, USA. *Geochimica et Cosmochimica Acta, 58*(22), 4955–4972. https://doi.org/10.1016/0016-7037(94)90224-0

Dou, Y., Yang, S., Liu, Z., Clift, P. D., Yu, H., Berne, S., & Shi, X. (2010). Clay mineral evolution in the central Okinawa Trough since 28 ka: Implications for sediment provenance and paleoenvironmental change. *Palaeogeography, Palaeoclimatology, Palaeoecology, 288*(1–4), 108–117. https://doi.org/10.1016/j.palaeo.2010.01.040

Fairbanks, R. G. (1989). A 17,000-year glacio-eustatic sea level record: Influence of glacial melting rates on the Younger Dryas event and deep-ocean circulation. *Nature, 342*(6250), 637–642. https://doi.org/10.1038/342637a0

Furukawa, M., Tokuyama, H., Abe, S., Nishizawa, A., & Kinoshita, H. (1991). Report of DELP 1988 cruises in the Okinawa Trough. *Bulletin of the Earthquake Research Institute, 66*, 17–36.

Govindaraju, L. (1989). 1989 Compilation of working values and sample description for 272 geostandards. *Geostandards Newsletter*, 13(Special Issue), 1–113.

Guo, Z. G., Yang, Z. S., Lei, K., Gao, L., & Qu, Y. H. (2001). The distribution and composition of suspended matters and their influencing factors in the central-southern area of Okinawa Trough and its adjacent shelf sea. *Oceanologia et Limnologia Sinica, 23*(1), 66–72.

Ho, K. S., & Chen, J. C. (1996). Geochemistry and origin of tektites from Penglei area, Hainan province, southern China. *Journal of Southeast Asian Earth Sciences, 13*(1), 61–72. https://doi.org/10.1016/0743-9547(96)00005-0

Hsu, S. C., Lin, F. J., Jeng, W. L., Chung, Y. C., Shaw, L. M., & Hung, K. W. (2004). Observed sediment fluxes in the southwestern most Okinawa Trough enhanced

by episodic events: Flood runoff from Taiwan Rivers and large earthquakes. *Deep Sea Research Part I: Oceanographic Research Papers, 51*(8), 979–997. https://doi.org/10.1016/j.dsr.2004.01.009

Hsu, S. C., Lin, F. J., Jeng, W. L., & Tang, T. Y. (1998). The effect of a cyclonic eddy on the distribution of lithogenic particles in the southern East China Sea. *Journal of Marine Research, 56*(4), 813–832. https://doi.org/10.1357/002224098321667387

Hsu, S. K. (2001). Lithospheric structure, buoyancy and coupling across the southernmost Ryukyu subduction zone: An example of decreasing plate coupling. *Earth and Planetary Science Letters, 186*(3-4), 471–478. https://doi.org/10.1016/S0012-821X(01)00261-8

Huh, C. A., Su, C. C., Wang, C. H., Lee, S. Y., & Lin, I. T. (2006). Sedimentation in the southern Okinawa Trough – Rates, turbidites and a sediment budget. *Marine Geology, 231*(1-4), 129–139. https://doi.org/10.1016/j.margeo.2006.05.009

Hung, J. J., Lin, C. S., Hung, G. W., & Chung, Y. C. (1999). Lateral transport of lithogenic particles from the continental margin of the southern East China Sea. *Estuarine, Coastal and Shelf Science, 49*(4), 483–499. https://doi.org/10.1006/ecss.1999.0520

Hu, S., Zeng, Z., Fang, X., Qi, H., Yin, X., Chen, Z., Li, X., & Zhu, B. (2019). Geochemical study of detrital apatite in sediment from the southern Okinawa Trough: New insights into sediment provenance. *Minerals, 9*(10), 619–639. https://doi.org/10.3390/min9100619

Jackson, M. L. (1975). *Soil chemical analysis: Advanced course*. University of Wisconsin.

Jeffery, G. H., & Hutchison, D. (1981). *Vogel's textbook of quantitative chemical analysis* (4th ed.). Longman.

Kao, S. J., Lin, F. J., & Liu, K. K. (2003). Organic carbon and nitrogen contents and their isotopic compositions in surficial sediments from the East China Sea shelf and the southern Okinawa Trough. *Deep Sea Research Part II: Topical Studies in Oceanography, 50*(6-7), 1203–1217. https://doi.org/10.1016/S0967-0645(03)00018-3

Lee, C. Y. (2002). Taiwan area groundwater monitoring network phase II project. *Hydrogeological investigation and research* (pp. 1–59). Research Report Commissioned by the Central Geological Survey, Ministry of Economic Affairs.

Lee, C. S., Shor, G. G. Jr., Bibee, L. D., Lu, R. S., & Hilde, T. W. C. (1980). Okinawa Trough: Origin of a back-arc basin. *Marine Geology, 35*(1-3), 219–241. https://doi.org/10.1016/0025-3227(80)90032-8

Lee, S. Y., Huh, C. A., Su, C. C., & You, C. F. (2004). Sedimentation in the Southern Okinawa Trough: Enhanced particle scavenging and teleconnection between the Equatorial Pacific and western Pacific margins. *Deep Sea Research Part I: Oceanographic Research Papers, 51*(11)1, 1769–1780. https://doi.org/10.1016/j.dsr.2004.07.008

Letouzey, J., & Kimura, M. (1985). Okinawa Trough genesis: Structure and evolution of the back-arc basin developed in a continent. *Marine and Petroleum Geology, 2*(2), 111–130. https://doi.org/10.1016/0264-8172(85)90002-9

Li, C., Francois, R., Yang, S., Barling, J., Darfeuil, S., Luo, Y., & Weis, D. (2016). Constraining the transport time of lithogenic sediments to the Okinawa Trough (East China Sea). *Chemical Geology, 445*, 199–207. https://doi.org/10.1016/j.chemgeo.2016.04.010

Li, C. S., Jiang, B., Li, A. C., Li, T. G., & Jiang, F. Q. (2009). Sedimentation rates and provenance analysis in the Southwestern Okinawa Trough since the mid-Holocene. *Chinese Science Bulletin, 54*(7), 1234–1242. https://doi.org/10.1007/s11434-009-0010-0

Li, W. R., Yang, Z. S., Wang, Q., Cao, L. H., Wang, Y. J., & Wang, X. L. (2001). Terrigenous transportation through canyon and sedimentation of submarine fan in the Okinawa Though. *Oceanologia et Limnologia Sinica, 32*(4), 371–380.

Lin, F. J., & Chen, J. C. (1983). Textural and mineralogical studies of sediments from the Southern Okinawa Trough. *Acta Oceanographica Taiwanica, 14*, 26–41.

Lin, K. L. (1992). *Sedimentary structure, texture and clay minerals of surficial sediments off northeastern Taiwan* (Master's thesis, Institute of Oceanography, National Taiwan University, Taiwan), 93 pp.

Lin, J. Y., Sibuet, J. C., Lee, C. S., Hsu, S. K., Klingelhoefer, F., Auffret, Y., Pelleau, P., Crozon, J., & Lin, C. H. (2009). Microseismicity and faulting in the southwestern Okinawa Trough. *Tectonophysics, 466*(3-4), 268–280. https://doi.org/10.1016/j.tecto.2007.11.030

Lou, J. Y., & Chen, A. C. T. (1996). A paleoenvironmental record during 7-21 Ka BP in the sediments off northern Taiwan. *La Mer, 34*(3), 237–245.

Luo, J. P. (2001). *Study on the structure and distribution of igneous rocks in the southern Okinawa Trough* (Master's thesis, Institute of Oceanography, National Taiwan University, Taiwan), 67 pp.

Meisel, T., Koeberl, C., & Ford, R. J. (1990). Geochemistry of Darwin impact glass and target rocks. *Geochimica et Cosmochimica Acta, 54*(5), 1463–1474. https://doi.org/10.1016/0016-7037(90)90169-L

Moore, D. M., & Reynolds, R. C. (1997). *X-ray diffraction and the identification and analysis of clay minerals* (2nd ed.). Oxford University Press.

Murphy, J., & Riley, J. P. (1962). A modified single solution method for the determination of phosphate in natural waters. *Analytica Chimica Acta, 27*, 31–36. https://doi.org/10.1016/S0003-2670(00)88444-5

Nyakairu, G. W. A., & Koeberl, C. (2001). Mineralogical and chemical composition and distribution of rare earth elements in clay-rich sediments from central Uganda. *Geochemical Journal, 35*(1), 13–28. https://doi.org/10.2343/geochemj.35.13

PerkinElmer. (1996). *Analytical methods for atomic absorption spectrometry*. PerkinElmer Analytical Instruments.

Roser, B. P., & Korsch, R. J. (1986). Determination of tectonic setting of sandstone-mudstone suites using SiO_2 and K_2O/Na_2O ratio. *The Journal of Geology, 94*(5), 635–650. https://doi.org/10.1086/629071

Shieh, Y. T., Wang, C. H., Chen, M. P., & Yung, Y. L. (1997). The last glacial maximum to Holocene environment changes in the southern Okinawa Trough. *Journal of Asian Earth Sciences, 15*(1), 3–8. https://doi.org/10.1016/S0743-9547(96)00075-X

Sibuet, J. C., Deffontaines, B., Hsu, S. K., Thareau, N., Formal, J. P. L., Liu, C. S., & The ACT Party. (1998). Okinawa Trough back-arc basin: Early tectonic and magmatic evolution. *Journal of Geophysical Research, 103*(B12), 30245–30267. https://doi.org/10.1029/98JB01823

Sibuet, J. C., Hsu, S. K., Shyu, C. T., & Liu, C. S. (1995). Structural and kinematic evolution of the Okinawa Trough back-arc basin. In B. Taylor (Ed.), *Back-arc basins: Tectonics and magmatism* (pp. 343–378). Plenum Press.

Sibuet, J.-C., Le Pichon, X., Lallemand, S., Foucher, J.-P., McKenzie, D., & Winterer, E. (1987). Back-arc extension in the Okinawa Trough. *Journal of Geophysical Research, 92*(B13), 41–14. https://doi.org/10.1029/JB092iB13p14041

Taylor, S. W., & McLennan, S. H. (1985). *The continental crust: Its composition and evolution* (p. 312). Blackwell.

Ujiie, H. (1994). Early Pleistocene birth of the Okinawa Trough and Ryukyu Island Arc at the northwestern margin of the Pacific: Evidence form Late Cenozoic planktonic foraminiferal zonation. *Palaeogeography, Palaeoclimatology, Palaeoecology, 108*(3–4), 457–474. https://doi.org/10.1016/0031-0182(94)90246-1

Ujiie, H., Tanaka, Y., & Ono, T. (1991). Late Quaternary paleoceanographic record from the middle Ryukyu Trench slope, northwest Pacific. *Marine Micropaleontology, 37*(1-2), 23–40. https://doi.org/10.1016/0377-8398(91)90008-T

Ujiie, H., & Ujiie, Y. (1999). Late Quaternary course changes of the Kuroshio Current in the Ryukyu Arc region, northwestern Pacific Ocean. *Marine Micropaleontology, 37*(1), 23–40. https://doi.org/10.1016/S0377-8398(99)00010-9

Wang, C. H., Chen, J. C., & Liu, K. K. (1985). Stable isotope records from Holocene deep-sea sediments off northeastern Taiwan. *Bulletin of the Institute of Earth Sciences, Academia Sinica, 5*, 59–66.

Zhu, B., & Zeng, Z. (2022). Detrital zircon provenance in the sediments in the Southern Okinawa Trough. *Journal of Marine Science and Engineering, 10*(2), 142–156. https://doi.org/10.3390/jmse10020142